QUARTERLY JOURNAL OF THE ROYAL METEOROLOGICAL SOCIETY
Q. J. R. Meteorol. Soc. **134**: 385–402 (2008)
Published online 2 April 2008 in Wiley InterScience
(www.interscience.wiley.com) DOI: 10.1002/qj.219

A method for quantifying the impacts and interactions of potential-vorticity anomalies in extratropical cyclones

R. Romero*

Grup de Meteorologia, Departament de Física, Universitat de les Illes Balears, Palma de Mallorca, Spain

ABSTRACT: The theory of potential vorticity (PV) allows us to describe the life cycle of mid-latitude baroclinic systems in terms of the individual impacts and interactions of distinct PV anomalies embedded in the background flow. PV anomalies associated with the undulating tropopause, the low-level thermal field, and key diabatic processes such as the latent-heat release within the cloudy systems of the cyclone, are often considered as evolving features regulated by their lateral and vertical mutual interactions and their interaction with the stratospheric high-latitude PV reservoir. Under some balance-flow assumptions, PV inversion can be used to quantify the contribution of the PV anomalies to the cyclone depth (or other attributes) at various stages of its life cycle (a *static* approach); but it is less clear how to diagnose with similar quantitative detail the various types of time-dependent interactions among the anomalies and mean flow that govern the processes of cyclogenesis and cyclolysis (a *dynamic* approach).

This paper presents a method that implements the concepts of 'PV thinking' quantitatively. The method first applies a piecewise PV-inversion scheme formulated according to the Charney nonlinear mass–wind-balance approximation. Then it combines a prognostic system of balance equations that are consistent with the applied inversion scheme with a factor-separation technique. By switching on and off the PV anomalies of interest, various flow configurations are generated, and the corresponding solutions to the prognostic equations can be algebraically combined to isolate the magnitude of both the individual and the synergistic effects of the PV anomalies on the spatial pattern of geopotential-height tendency (and vertical motion) around the cyclone, with low computational cost.

The potential of the method to elucidate the relative importance of physically-meaningful PV anomalies for the growth or decay of baroclinic systems is illustrated for the intense Mediterranean cyclone of 10–12 November 2001, using the NCEP meteorological grid analyses at 12 h intervals.

The upper-level PV anomalies contributed very significantly during the whole life cycle of this Mediterranean cyclone. Surface thermal anomalies were fundamental during the development period, and induced the general northeastward movement of the system during the later stages. During the mature stage of the cyclone, the interaction between the two types of anomalies became the dominant effect. All other contributions, including the individual and synergistic effects of diabatically-generated PV, were generally most relevant during this mature stage.

KEY WORDS potential-vorticity anomalies; PV thinking; extratropical cyclones; western Mediterranean

Received 7 September 2007; Revised 3 December 2007; Accepted 21 January 2008

1. Introduction

Since the seminal paper of Hoskins *et al*. (1985), the use of potential vorticity (PV) to analyse the genesis and evolution of synoptic-scale systems has become very popular in meteorology. In isentropic coordinates, the two powerful principles of conservation (that PV behaves as a tracer of atmospheric motion under adiabatic and frictionless conditions) and invertibility (that positive (negative) PV anomalies or warm (cold) surface potential-temperature anomalies (Thorpe, 1985) induce characteristic cyclonic (anticyclonic) flow patterns) can be readily combined to develop a conceptually-elegant framework that extends the capabilities of the more traditional quasi-geostrophic (QG) theory for explaining the dynamics of mid-latitude circulation systems. This method of dynamical analysis, referred to as 'PV thinking' by Hoskins *et al*. (1985), has been applied to explain many kinds of problems, such as (see Bluestein (1993) for relevant references):

- the pattern of vertical motion under an approaching upper-level disturbance or a surface thermal anomaly embedded in the westerlies;
- the movement of weather systems according to certain modes of lateral interaction among PV anomalies and background flow (e.g. vortex–vortex interaction, vortex retrogression, background-flow advection of vortices (Hakim *et al*, 1996));
- zonal, meridional and vertical Rossby-wave propagation;
- the motion of surface cyclones and anticyclones on level and sloped terrain;

* Correspondence to: R. Romero, Departament de Física, Universitat de les Illes Balears, 07122 Palma de Mallorca, Spain.
E-mail: Romu.Romero@uib.es

- barotropic instability;
- the growth of baroclinic-wave–cyclone systems, including the feedback of clouds and precipitation into the dynamics of cyclones via the release of latent heat, a source of PV anomalies (Davis and Emanuel, 1991).

PV diagnostics have been particularly beneficial for gaining insight into the processes involved in extratropical cyclogenesis governed by baroclinic dynamics. In contrast to the celebrated theoretical explanation for cyclogenesis in terms of baroclinic instability – that is, the growth of an initially small-amplitude disturbance on an unstable basic state (Charney, 1947; Eady, 1949) – the PV-based approach examines whether the structure of a finite-amplitude PV perturbation initially present in the upper troposphere or in the lower boundary, rather than the stability characteristics of the basic state, will determine development at the surface (e.g. Davis and Emanuel, 1991). In this regard, it should be noted that large-amplitude upper-level disturbances are often present before the baroclinic growth of the wave–cyclone system commences (e.g. Sanders, 1986, 1988).

Extratropical cyclogenesis is the best paradigm for mutual reinforcement between anomalies of different origin. The vertical interaction between the upper-level wave-like PV anomaly and the potential-temperature field along the lower boundary is fundamental to explaining the baroclinic growth of the disturbance (Hoskins *et al*, 1985): as the upper-level cyclonic PV anomaly arrives over a region of significant low-level baroclinicity, its induced circulation will promote warm advection east of it, creating a warm anomaly at the surface, which in turn will induce its own cyclonic circulation that is felt just to the east of the upper-level positive PV anomaly, thus contributing to its amplification by the southward advection of the high PV values found at higher latitudes: a positive-feedback mechanism that will be reflected as the growth of the wave–cyclone system in this idealized dry atmosphere. For the real, moist atmosphere, the generation of low-level PV anomalies is due not only to advection but also to differential surface heating and condensation of water vapour in the atmospheric column. The role of latent-heat release in accelerating the growth of the disturbance is well recognized, and this factor has been included explicitly in the PV framework by some authors (e.g. Davis and Emanuel, 1991).

Several studies have applied nonlinear-balance PV-inversion algorithms to diagnose the life cycle of extratropical cyclones with sub-synoptic detail. Commonly, these studies implement an attribution methodology: first, PV anomalies of interest are isolated from the total PV field at particular stages of the cyclone life; then the PV inversion is applied to retrieve the horizontal-velocity and temperature fields induced by the anomalies (e.g. Davis, 1992a; Hakim *et al*, 1996; Huo *et al*, 1999a). Unlike the QG dynamics, in which the attribution method is conceptually simple because of the linear form of the PV definition, in the more accurate nonlinear balance diagnosis no unique flow and mass fields exist in association with a specific PV anomaly. Various criteria can be applied to partition the flow into the contributions induced by the anomalies in the nonlinear system (Davis, 1992b). In spite of this ambiguity, the reliability of the attribution approach has been clearly demonstrated (Davis, 1992b; Thorpe, 1997).

Retrieval of horizontal velocity and temperature distributions induced by the anomalies, and in some cases vertical motion field through the involvement of an omega equation (see, for example, Clough *et al*. (1996) for the QG system, and Ziemianski and Thorpe (2000) for the nonlinear system) merely provides a 'static' solution to the attribution problem: instantaneous contributions of the PV anomalies to the cyclone structure (in terms of geopotential, temperature and wind distributions) are perfectly quantified, but the role of the PV anomalies in the subsequent evolution of the baroclinic disturbance can only be qualitatively inferred after invoking the conservation principle and projecting in time the new PV field, which is continuously reshaped by all kinds of lateral and vertical interactions among the anomalies (e.g. Huo *et al*, 1999a).

Some authors have combined piecewise inversion schemes with numerical forecast models in the design of initial-value problems, where the effects of incorporating, modifying or removing PV perturbations (i.e. a certain amount of balanced flow) in the model initial conditions on the subsequent forecast are investigated (e.g. Huo *et al*, 1998; Huo *et al*, 1999b; Romero, 2001; Martín *et al*, 2007). In this case the integrated effects of the initial PV perturbations can be exactly isolated, but the nature and amount of the interactions between the PV anomalies that govern the cyclone evolution are even more obscure than in the static approach.

In this study we devise a 'dynamic' approach that allows us to isolate quantitatively the impacts and interactions of the PV anomalies during the life cycle of the cyclone. The method utilizes the so-called factor-separation technique (Stein and Alpert, 1993), applied to the prognostic system of balance equations described in Davis and Emanuel (1991) in association with their nonlinear-balance piecewise PV-inversion technique. We emphasize the dynamic characteristics of the method, resulting from diagnostics of the geopotential-height tendency field and thus of the processes governing the cyclogenesis, cyclone propagation and cyclolysis. The fact that it allows us to quantify both the individual and the synergistic contributions of the PV anomalies to the tendency field is of major relevance: the PV theory of the baroclinic disturbance is easily established, and the various dynamical processes participating in that theory can be hierarchically organized as a function of the cyclone stage. An additional advantage is the low computational cost of the approach, since it does not involve numerical simulations. Of course, this also means that physical processes other than those included in our balance dynamics cannot be accounted for, but these are believed to play only a secondary role in mid-latitude cyclones (e.g. Ahmadi-Givi *et al*, 2004). The capabilities of the new method will be illustrated through the analysis of the strong cyclogenesis event that affected the western Mediterranean region on 10–12 November 2001.

The paper is structured as follows. A synoptic overview of the November 2001 super-storm is provided in Section 2. The relevant dry and moist PV anomalies of the episode are defined in Section 3, and their contributions to the surface cyclone are analysed according to the results of piecewise PV inversion (the static approach). In Section 4, the prognostic system of balance equations is combined with the factor-separation technique to develop the dynamic approach, and this tool is used to diagnose in the light of 'PV thinking' the impacts and interactions of the anomalies in our event. Conclusions and prospects are presented in Section 5.

2. The Mediterranean cyclone of 10–12 November 2001

The Mediterranean basin is recognized as one of the world's major cyclogenetic areas (Pettersen, 1956; Radinovic, 1987), and much of the high-impact weather affecting the Mediterranean countries (notably strong winds and heavy precipitation) has been statistically associated with the near presence of a distinct cyclonic signature (e.g. Jansá *et al*, 2001). Cyclones can range in size from synoptic to mesoscale, and in type from pure baroclinic systems to orographically or diabatically modulated disturbances, and their peak occurrences and notorious consequences have been clearly linked to the presence of prominent orographic systems surrounding the Mediterranean Sea. Various airflow–barrier interactions can promote shallow lee cyclones (Genovés and Jansá, 1991), or affect classical baroclinic development, usually favouring and focusing cyclogenesis (Speranza *et al*, 1985). Many violent windstorms result from a combination of cyclonic winds and local topographic effects induced by downslope or channelling mechanisms, such as the Mistral, Tramontane, Scirocco, Ethesian and Bora (Reiter, 1975). The orography also becomes crucial in many flash-flood environments, when a moist low-level jet organized by a near or distant cyclone impinges over the coastal ridges (Martín *et al*, 2007).

In spite of the relatively low latitude of the Mediterranean region, some of the baroclinic developments can be so fast as to reach the category of 'meteorological bombs' (Conte, 1986; Homar *et al*, 2000). The intense cyclone of 10–12 November 2001 did not reach that category, but the social impacts of this cyclone produced by wind and rain in the western Mediterranean regions have no parallel in recent decades. More than 600 people were killed and many left homeless in Algiers (Algeria), where 262 mm of rain falling in 24 h during the North African growth phase of the disturbance produced catastrophic flooding. Floods also occurred during that phase in Morocco. The Balearic Islands in Spain were affected during the mature phase of the storm, with unprecedented consequences, including four casualties, nearly half a million trees uprooted, up to 60% sand removal in north-facing beaches, more than 300 mm of rainfall in the mountains, and subsequent floods, serious interruptions of traffic, electricity supply and telephonic communications, and damage to private property exceeding 100 million euros. Other coastal areas of Spain, southern France and Italy were also hit by the significant oceanic surge and sea waves originating from the cyclone (before the electricity disruption in the Balearics, sustained winds and wind gusts in excess of 30 $\mathrm{ms^{-1}}$ and 42 $\mathrm{ms^{-1}}$ respectively were recorded, and wave heights on open sea are estimated to have exceeded 10 m). The devastating nature of this storm has motivated many studies since then (e.g. Jansá and Romero, 2003), although it should be mentioned that the cyclone itself was reasonably well forecast by a number of numerical models operating in the region. The strong predictability of the event was tied to the governing action of the large-scale flow evolution.

The life cycle of the storm (Figure 1) resembles the synoptic evolution of another deep cyclone of African origin studied by Homar *et al*. (2000). In fact, these two events are the most severe cyclones to have affected the Balearics in the last 30 years. The surface cyclone originated over North Africa, in a region of marked baroclinicity (Figure 1(b)) preceded by a significant cold-air intrusion at upper levels from north central Europe towards Iberia and Morocco (see the cold upper-level trough in Figure 1(a)). During this incipient phase on 9–10 November, flash floods occurred in Algeria and Morocco. As the cyclone evolved northeastwards into the western Mediterranean basin, the central pressure continued to deepen and an appreciable pressure gradient developed around its core, leading to the mature, most intense state of the cyclone at around 00 UTC on 11 November (Figure 1(d)). At this time, the warm- and cold-front signatures in the low-level thermal field are both very clear, and occlusion is suggested near the tip of the warm-air surge from North Africa induced by the circulation. Meanwhile, the upper-level circulation adopted cut-off characteristics, and two geopotential-height minima are visible in the NCEP analysis, located to the west and east of the Strait of Gibraltar at 00 UTC on 11 November (Figure 1(c)). Most of the rainfall, and the main wind-induced damage in the Balearic Islands (located in the centre of the western Mediterranean), occurred during the mature phase of the cyclone. The meteorological analyses at 00 UTC on 12 November (Figure 1(e,f)) correspond to the decay of the disturbance: the low-pressure system filled as it progressed further northwards and the thermal gradient weakened appreciably (Figure 1(f)), and interestingly the two upper-level embedded disturbances rotated cyclonically about each other as the large-scale parent trough entered the western Mediterranean (Figure 1(e)).

Although the primary role of baroclinic instability is clearly established according to the previous synoptic evolution, the high precipitation potential of this cyclone and the massive cloudy structures that could be observed on the satellite images during the oceanic phase of the

DOI: 10.1002/qj

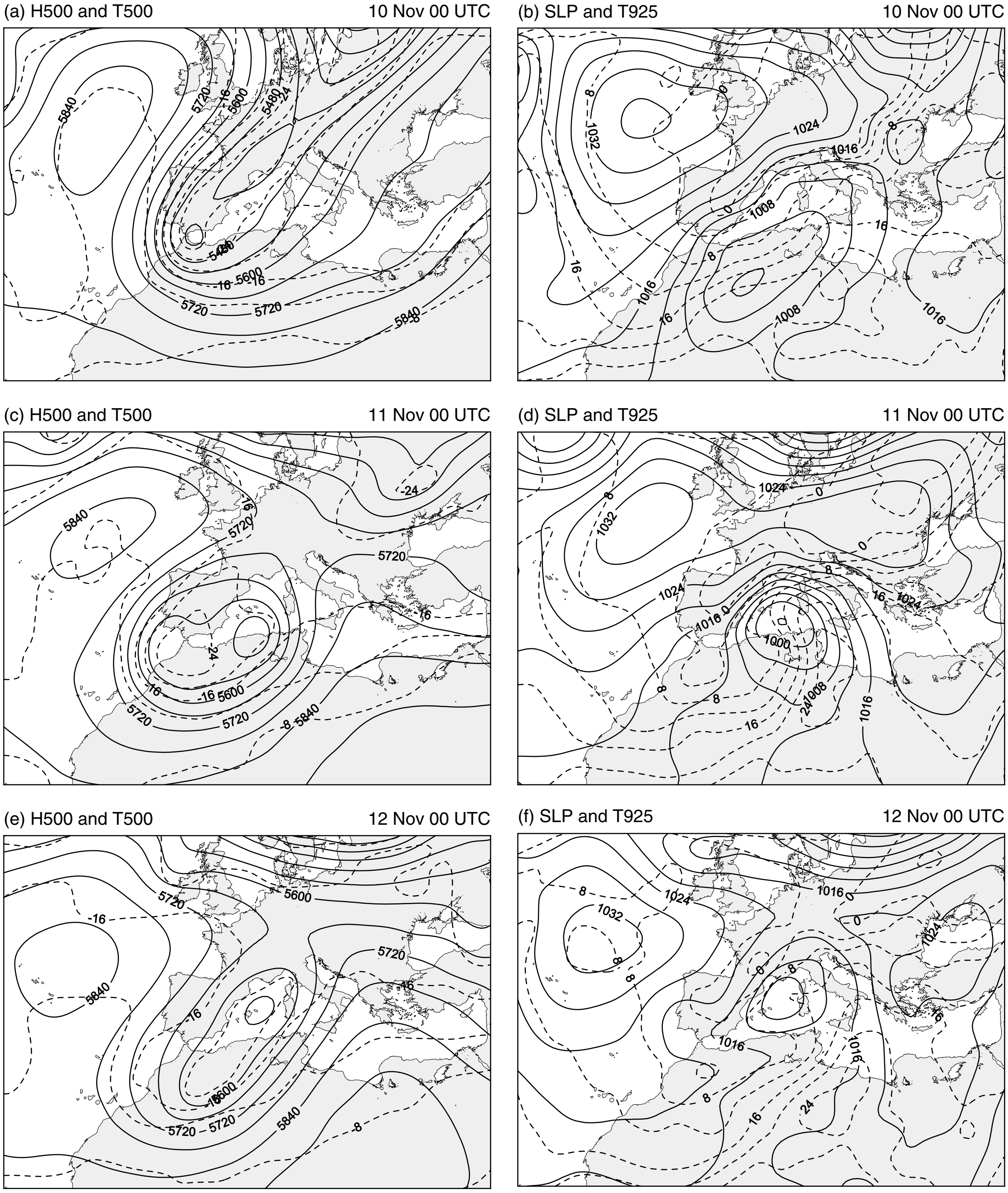

Figure 1. Synoptic situation, extracted from the NCEP analyses, at 00 UTC on: (a,b) 10 November 2001; (c,d) 11 November 2001; (e,f) 12 November 2001. The following fields are shown: (a,c,e) geopotential height at 500 hPa (solid lines, contour interval 60 gpm) and temperature at 500 hPa (dashed lines, contour interval 4 °C); (b,d,f) sea-level pressure (solid lines, contour interval 4 hPa) and temperature at 925 hPa (dashed lines, contour interval 4 °C).

storm (Figure 2) suggest that condensational latent-heat release could also have played a role in the cyclone development. Therefore, the contributions to the storm of diabatically-generated PV within the cloud systems will be explicitly considered in the following analyses.

3. Role of dry and moist PV anomalies: static approach

This study deals with the attribution of static and dynamic effects to certain anomalies of the PV field. Accordingly, the methodology first requires a choice among the available PV formulations, and then some criteria for defining the anomalies.

The Ertel PV (Rossby, 1940; Ertel, 1942) is used. This is defined as:

$$q = \frac{1}{\rho}\boldsymbol{\eta} \cdot \nabla\theta, \tag{1}$$

where ρ is the density, η is the absolute-vorticity vector, and θ is the potential temperature. When defining

DOI: 10.1002/qj

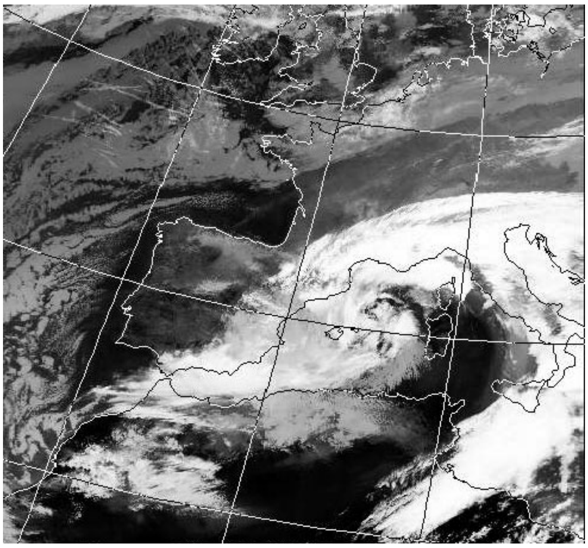

Figure 2. Infrared image on 11 November 2001 at 13:29 UTC, corresponding to channel 4 of the NOAA satellite.

anomalies in a flow pattern, it is common practice to compare the instantaneous state with a time-mean state. We will follow this approach, and for the cyclone of 10–12 November 2001 a reference state is built as the seven-day time average of the fields for the period from 00 UTC on 7 November to 00 UTC on 14 November. The difference between the instantaneous distribution of Ertel PV q and its time-mean distribution $\overline{q}$ will determine the PV perturbation q':

$$q = \overline{q} + q'. \tag{2}$$

In addition, the perturbation potential temperature θ' at the top and bottom boundaries of the three-dimensional domain can be regarded as equivalent to a concentrated PV perturbation contained in these thin layers.

Next, a collection of PV anomalies q_n can be arbitrarily defined from q' in a piecewise manner:

$$q' = \sum_{n=1}^{N} q_n. \tag{3}$$

Although the number and type of PV anomalies in Equation (3) may be as large and complex as we wish, we will consider a simple but physically-meaningful decomposition of q' that is appropriate for interpreting the baroclinic event according to the processes emphasized by 'PV thinking'. Three unique anomalies are defined (see Table I): *ULev* is associated with the undulating tropopause, and will contain the PV perturbation above 700 hPa plus the θ' field at the upper boundary, located at 100 hPa; *LLev* represents the surface baroclinicity, since it is composed of θ' at the bottom boundary (1000 hPa) and the lower-level interior PV perturbation, up to 700 hPa; *Diab* is expressed as the positive PV perturbation below 500 hPa in areas with greater than 70% relative humidity. The latter is defined to account for the lower-tropospheric PV anomalies associated with condensational heating. A subsaturated threshold value of 70% is chosen for two reasons: first, saturated areas are seldom captured in large-scale grid analyses such as the ones used in this study; and secondly, this value allows us to include PV that may advect out of the precipitation region. Wherever the interior q' is assigned to *Diab* according to the above definition, it will be removed from *ULev* or *LLev*. Thus we can refer unambiguously to *ULev* and *LLev* as the dry PV anomalies, associated with the baroclinic processes, and to *Diab* as a moist anomaly, related to the diabatic contribution of clouds and precipitation. It is important to note that at any point of the interior domain, the sum of *ULev*, *LLev* and *Diab* equals the total perturbation field q', as well as the total θ' field at the boundaries. Note also that *ULev* and *LLev* incorporate both positive and negative PV anomalies (e.g. upper-level troughs and ridges and warm and cold surface anomalies, respectively), whereas *Diab* is positive everywhere. A further split of *ULev* and *LLev* into their positive and negative pieces could reasonably be considered for a more detailed analysis of the event.

The three PV anomalies have been calculated using the NCEP grid meteorological analyses remapped over the domain of interest via a Lambert conformal map projection. The same grid analyses, available on standard isobaric surfaces at 12 h intervals with a horizontal resolution of 2.5°, have been used in the remainder of this study. The patterns of *ULev*, *LLev* and *Diab* along the period of the mature storm are shown in Figure 3 for some specific isobaric levels. The evolving character of the three anomalies is quite evident, and they can easily be tracked (in a cyclonic sense) across the three times presented – especially *ULev*. The relevant signatures emphasized in the last section, such as the two upper-level embedded disturbances, the marked low-level baroclinicity, and the massive cloud formation over the western Mediterranean, are well identified on the PV charts (see, respectively, *ULev*, *LLev* and *Diab* on Figure 3(b)).

The method employed to derive the impacts and interactions of the PV anomalies is based on the invertibility principle, which allows us to calculate a balanced flow associated with each anomaly. The piecewise PV-inversion technique of Davis and Emanuel (1991) is applied for this purpose. This technique is summarized

Table I. The PV anomalies used in this study, associated with mid-to-upper-tropospheric levels (*ULev*), lower-tropospheric levels (*LLev*), and condensational diabatic processes (*Diab*).

PV anomaly	Definition
ULev	PV perturbation above 700 hPa
LLev	surface thermal anomaly and PV perturbation below 700 hPa
Diab	positive PV perturbation below 500 hPa in areas with relative humidity exceeding 70%

DOI: 10.1002/qj

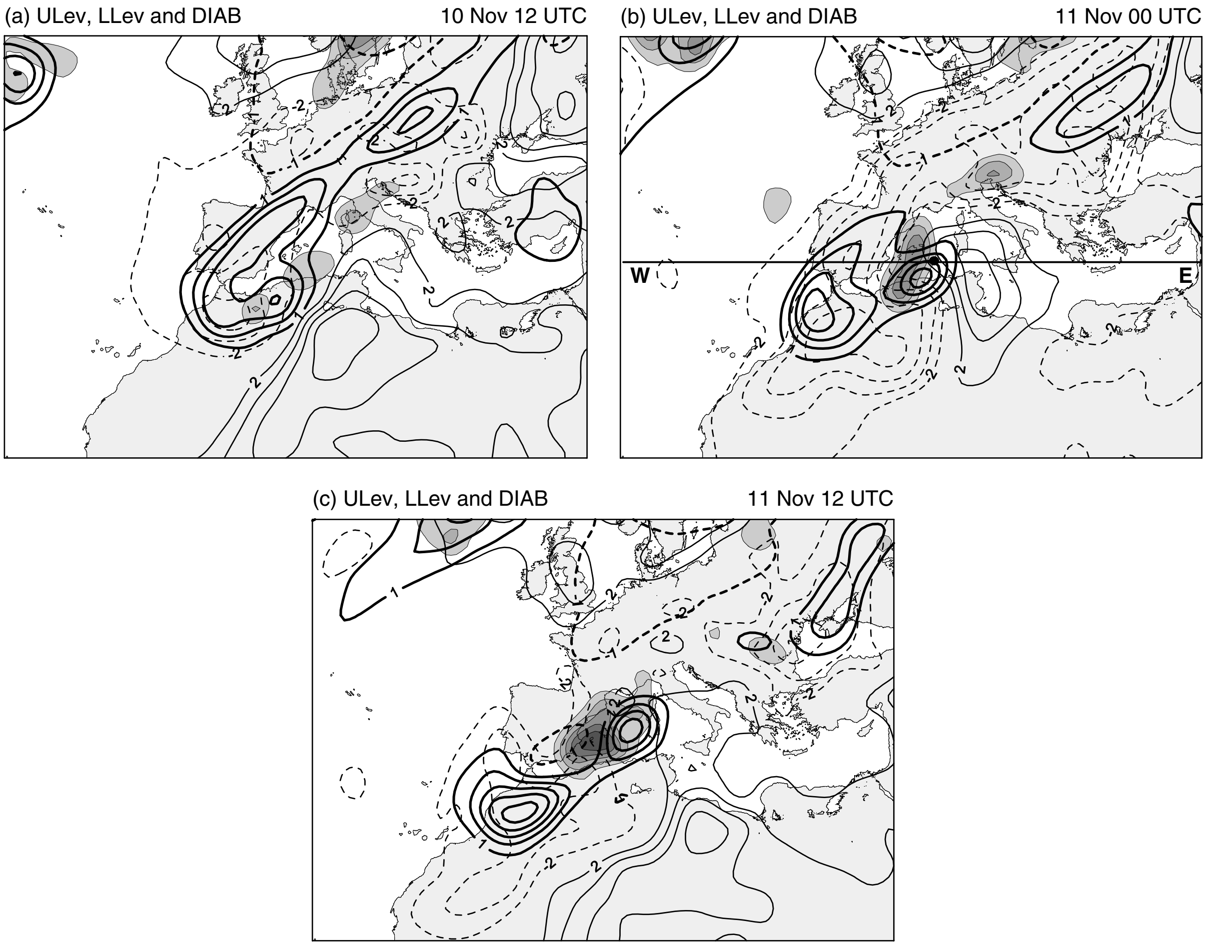

Figure 3. The PV anomalies *ULev*, *LLev* and *Diab* (see Table I), at: (a) 12 UTC on 10 November; (b) 00 UTC on 11 November; (c) 12 UTC on 11 November. The *ULev* field is shown at 300 hPa using thick contours (solid and dashed lines indicate positive and negative values of the PV anomaly, respectively, starting at 1 PVU and −1 PVU, every 1.5 PVU); *LLev* is shown by means of the thermal boundary condition at 1000 hPa using thin contours (solid and dashed lines indicate positive and negative values of the temperature anomaly, respectively, starting at 2°C and −2°C, every 2°C); *Diab* is shown at 700 hPa as shaded contours, starting at 0.1 PVU, every 0.1 PVU. The west–east line in panel (b) indicates the vertical cross section analysed in Figure 4, and the central dot indicates the position of the surface cyclone at that time.

below. The same equations, as well as some others, can be found in Davis and Emanuel (1991), but we formulate them using map coordinates (x, y) instead of geographical coordinates.

3.1. Piecewise PV inversion

The method starts with the calculation of a balanced flow, described by the geopotential ϕ and the stream function ψ, from the instantaneous distribution of Ertel PV q, given by Equation (1). The balance assumption made herein follows the Charney (1955) nonlinear balance equation, also called the Bolin–Charney equation in recognition of its simultaneous construction by Bolin (1955). This balance assumption is quite accurate even for meteorological systems characterized by large Rossby numbers. It is expressed as:

$$\nabla^2\phi = \nabla \cdot f\nabla\psi + 2m^2\left\{\frac{\partial^2\psi}{\partial x^2}\frac{\partial^2\psi}{\partial y^2} - \left(\frac{\partial^2\psi}{\partial x\partial y}\right)^2\right\}, \quad (4)$$

where f is the Coriolis parameter and m denotes the map-scale factor of the projection used. The other diagnostic relation necessary for the inversion of ϕ and ψ is given by the approximate form of Equation (1) resulting from the hydrostatic assumption and the same scale analysis used to derive Equation (4), namely, that the irrotational component of the wind is very small relative to the non-divergent wind:

$$q = \frac{g\kappa\pi}{p}\left\{(f + m^2\nabla^2\psi)\frac{\partial^2\phi}{\partial\pi^2} - m^2\left(\frac{\partial^2\psi}{\partial x\partial\pi}\frac{\partial^2\phi}{\partial x\partial\pi} + \frac{\partial^2\psi}{\partial y\partial\pi}\frac{\partial^2\phi}{\partial y\partial\pi}\right)\right\} \quad (5)$$

where p is the pressure, g is the gravity, $\kappa = R_d/C_p$ is the ratio of the gas constant to the isobaric heat capacity for dry air, and the vertical coordinate π is the Exner function $C_p(p/p_0)^\kappa$, with $p_0 = 1000\,\text{hPa}$.

The finite-difference form of the closed system described by Equations (4) and (5) is solved for the unknowns ϕ and ψ given q, using an iterative process that continues until convergence of the solutions is reached (refer to Davis and Emanuel (1991)

DOI: 10.1002/qj

for the details). Neumann-type conditions ($\partial\phi/\partial\pi = f\partial\psi/\partial\pi = -\theta$, where θ is potential temperature) are applied on the top and bottom boundaries, and Dirichlet conditions on the lateral boundaries. The latter are supplied by the observed geopotential and a stream function calculated by matching its gradient along the edge of each isobaric surface to the observed normal wind component, which is first slightly modified to force no net divergence in the domain.

Next, a balanced time-mean flow $(\overline{\phi}, \overline{\psi})$ is inverted from the previously-defined reference state $\overline{q}$, using equations identical to (4) and (5) except that all dependent variables are mean values and the mean potential temperature $\overline{\theta}$ is used for the top and bottom boundary conditions. The perturbation flow (ϕ', ψ') is given by:

$$(\phi, \psi) = (\overline{\phi}, \overline{\psi}) + (\phi', \psi'). \tag{6}$$

Finally, following the decomposition of the PV perturbation field q' in Equation (3), we are interested in obtaining that part of the flow (ϕ_n, ψ_n) associated with each PV anomaly q_n, and we also require

$$\left.\begin{array}{l} \phi' = \sum\limits_{n=1}^{N} \phi_n \\ \psi' = \sum\limits_{n=1}^{N} \psi_n \end{array}\right\}. \tag{7}$$

As discussed in Davis (1992b), there is no unique way to define a relationship between (ϕ_n, ψ_n) and q_n because of the nonlinearities present in Equations (4) and (5). Here, we adopt the linear method of Davis and Emanuel (1991), derived after substitution of the expressions (2) and (6) and the summations (3) and (7) in Equations (4) and (5) and equal partitioning of the nonlinear term among the other two linear terms that result from each nonlinearity in the equations (see Davis and Emanuel (1991) for details). The resulting linear closed system for the nth perturbation is given by:

$$\nabla^2\phi_n = \nabla\cdot f\nabla\psi_n + 2m^2\left(\frac{\partial^2\psi^*}{\partial x^2}\frac{\partial^2\psi_n}{\partial y^2} + \frac{\partial^2\psi^*}{\partial y^2}\frac{\partial^2\psi_n}{\partial x^2} - 2\frac{\partial^2\psi^*}{\partial x\partial y}\frac{\partial^2\psi_n}{\partial y\partial x}\right), \tag{8}$$

and

$$q_n = \frac{g\kappa\pi}{p}\left\{(f + m^2\nabla^2\psi^*)\frac{\partial^2\phi_n}{\partial\pi^2} + m^2\frac{\partial^2\phi^*}{\partial\pi^2}\nabla^2\psi_n - m^2\left(\frac{\partial^2\phi^*}{\partial x\partial\pi}\frac{\partial^2\psi_n}{\partial x\partial\pi} + \frac{\partial^2\phi^*}{\partial y\partial\pi}\frac{\partial^2\psi_n}{\partial y\partial\pi}\right) - m^2\left(\frac{\partial^2\psi^*}{\partial x\partial\pi}\frac{\partial^2\phi_n}{\partial x\partial\pi} + \frac{\partial^2\psi^*}{\partial y\partial\pi}\frac{\partial^2\phi_n}{\partial y\partial\pi}\right)\right\}, \tag{9}$$

where $(\cdot)^* = \overline{(\cdot)} + \frac{1}{2}(\cdot)'$.

Equations (8) and (9) are solved for the three interior PV anomalies *ULev*, *LLev* and *Diab* every 12 h during the life cycle of the storm, from 00 UTC on 10 November to 12 UTC on 12 November. With respect to the boundary conditions, the θ' field associated to each anomaly is used for the top and bottom Neumann-type boundary conditions; at the lateral boundaries, the perturbation geopotential and stream function above and below 700 hPa are used for *ULev* and *LLev*, respectively, whereas homogeneous boundary conditions for ϕ_n and ψ_n are assumed for *Diab*. The specific choice of the lateral boundary conditions should not be critical to the inverted fields over the western Mediterranean region, located in the central part of the domain (see Figure 3).

3.2. Results of the static approach

An example of the inverted fields, corresponding to the mature phase of the storm, is presented in Figure 4. This shows, along the west–east cross section indicated in Figure 3(b), the geopotential-height perturbation due to the three PV anomalies. Both height deficit (i.e. cyclonic vorticity) and height increase (anticyclonic vorticity) can be found in connection with the dry PV anomalies, thanks to their double signed pattern; perturbations of both signs alternate across the whole domain following the synoptic wave-train structure. Since the moist *Diab* anomaly is positive-definite, it only produces negative height perturbations, essentially in the form of a localized cyclonic vortex over the area of influence of the cyclone. As for the perturbations of other fields, such as temperature, static stability and horizontal wind, the height perturbation is maximum at mid-to-upper-tropospheric levels for *ULev* and at lower-tropospheric levels for *LLev* and *Diab*, because of the different source regions of the PV anomalies. In all cases, however, the induced perturbation is expanded throughout much of the atmospheric column

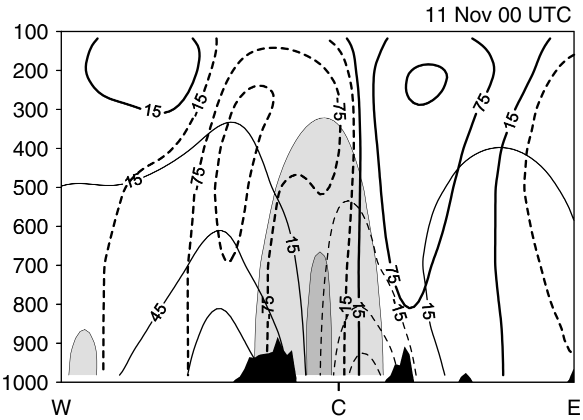

Figure 4. Vertical cross section, along the west–east line shown in Figure 3(b), of the PV-inverted geopotential-height perturbation field at 00 UTC on 11 November. Thick contours represent the field inverted from *ULev* (positive and negative values in continuous and dashed lines respectively, starting at 15 m and −15 m, every 60 m). Thin contours represent the field inverted from *LLev* (positive and negative values in continuous and dashed lines respectively, starting at 15 m and −15 m, every 30 m). Shaded contours represent the field inverted from *Diab* (contours every 30 m, starting at −15 m). The letter C at the bottom of the figure indicates the position of the cyclone.

(as well as horizontally): a natural consequence of the Laplacian operators involved in Equations (8) and (9).

A significant negative height contribution results from each PV anomaly over the area of the surface cyclone (letter C in Figure 4); these cooperate with each other to explain the intense barometric depression. The precise contribution of each anomaly to the surface low can be quantified in terms of the height perturbation at 1000 hPa; the results are plotted in Figure 5 for the complete life cycle of the storm. It can be seen that the North African cyclogenesis phase that occurred during the early hours of 10 November can be almost entirely attributed to the upper-level PV anomaly. Over the following hours, the *ULev* contribution starts to diminish while the *LLev* and *Diab* negative height perturbations over the cyclone centre increase in magnitude. At the time of the cyclone's peak intensity (11 November, 00 UTC), the three contributions attain similar values. Later, only the moist PV anomaly increases its negative contribution, while the *LLev*-induced perturbation gradually loses its identity over the low centre and *ULev* even acts to fill the cyclone (i.e. induces a positive height perturbation). Therefore, the decay phase of the storm during 12 November can be interpreted, in the perspective of PV inversion, as a lack of effective cooperation between the three PV anomalies.

To some extent, the early stage of the episode shown in Figure 5 describes the expected evolution of a type B extratropical cyclogenesis according to the twofold classification scheme of Pettersen and Smebye (1971): there is strong forcing by a pre-existing upper-level disturbance that controls the initial development, and the subsequent growth occurs in response to the cooperative interaction between the upper-level PV anomaly and the lower-level baroclinic zone. However, the cyclogenetic dynamics of the November 2001 case appear to be significantly modulated by the action of strong mid-level latent heating, an aspect not accounted for in the previous dry conceptual model.

The above PV-inversion results only provide a static depiction of the cyclogenesis–cyclolysis process, in the sense that only the contributions to the instantaneous cyclone intensity by the selected PV anomalies can be quantitatively diagnosed. Within the framework of PV theory, it would be illuminating to isolate with a similar degree of detail the true impact of the PV anomalies on the cyclone behaviour (i.e. on changes in its growth, decay, size, trajectory or shape), by means, for example, of the induced surface-pressure tendency and vertical motion. More importantly, it would be useful to split the contribution of each PV anomaly among its individual effects and the effects produced by its interaction with the other PV features or the mean flow. We may refer to this new perspective as a 'dynamic' approach to the PV-based diagnosis of cyclones. We will now proceed to develop this idea.

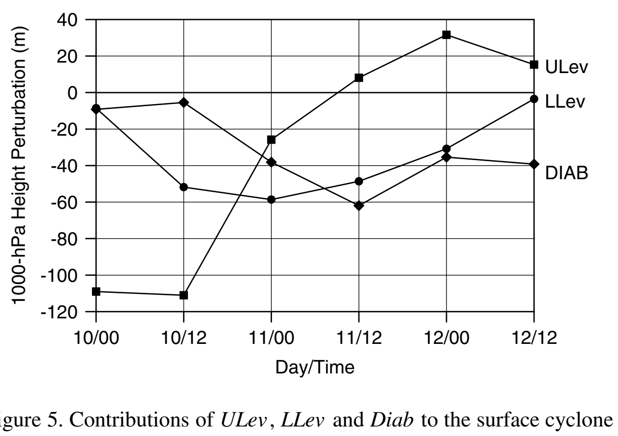

Figure 5. Contributions of *ULev*, *LLev* and *Diab* to the surface cyclone intensity, based on the PV-inverted 1000 hPa geopotential-height perturbation at the centre of the cyclone, every 12 h from 00 UTC on 10 November to 12 UTC on 12 November.

4. Quantifying the impacts and interactions of PV anomalies: dynamic approach

A first attempt towards identifying the nature and strength of the existing interactions between the anomalies might consist of calculating the horizontal advection of these anomalies by the PV-inverted flows derived in Section 3. Particularly relevant for understanding the baroclinic process are the effects of the PV anomalies on the lower-level thermal field and upper-level PV. Figures 6 and 7 show, respectively, the advection of these two fields induced by the *Mean* flow and by the PV anomalies *ULev*, *LLev* and *Diab*, on 11 November at 00 UTC. For the sake of brevity, several interactions appear combined in these introductory results. Specifically, the advected fields in both figures correspond to total fields, so in fact they are composed of more than one of the available *Mean*, *ULev*, *LLev* and *Diab* components. For instance, it is clear that the upper-level PV field shown as continuous lines in Figure 7 comprises both *Mean* and *ULev* PV components.

The results reveal lateral and vertical interactions of significant magnitude over the Mediterranean area, especially during the first (not shown) and mature phases of the cyclone. As an example, on 11 November at 00 UTC the *Mean* flow helps the North African thermal wave to propagate eastwards (Figure 6(a)), and *ULev* is the main factor responsible for the amplification of the warm thermal anomaly over the western Mediterranean (Figure 6(b)). The *LLev* PV anomaly contributes to both mechanisms – wave propagation and wave amplification (Figure 6(c)) – while the *Diab*-induced flow appears to exert only a minor influence on the thermal field (Figure 6(d)). With regard to the effects on the upper-level PV, the *Mean* flow again induces a progression of the disturbance towards the east (Figure 7(a)), but interestingly the *ULev*-induced flow acts in the opposite direction and induces a retrogression of the PV signature (Figure 7(b)), thus helping to reduce the mobility of the cyclonic system. The action of *LLev* and *Diab* on the upper-level PV is essentially a progressive one, similar to the *Mean* pattern, although an order of magnitude weaker

DOI: 10.1002/qj

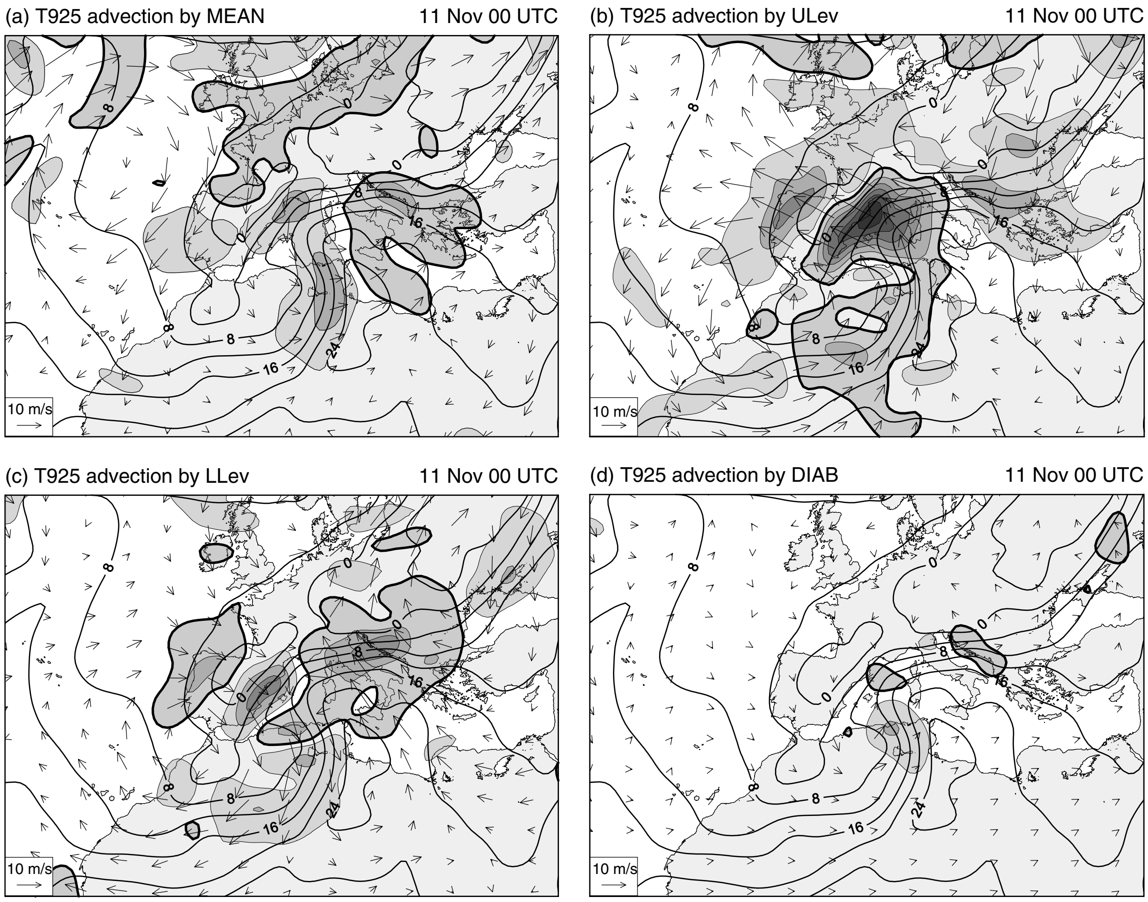

Figure 6. Temperature advection at 925 hPa at 00 UTC on 11 November, produced by: (a) the *Mean* flow; (b) the *ULev*-inverted flow; (c) the *LLev*-inverted flow; (d) the *Diab*-inverted flow. The advection field is shown as shaded for cold advection, and shaded within thick-line-highlighted regions for warm advection, starting at −2 °C/12 h and 2 °C/12 h respectively, with a contour interval of 5 °C/12 h. The temperature field and the PV-inverted advective flow at 925 hPa are also shown using continuous lines (in °C) and wind vectors (see reference vector at the bottom-left of each panel).

(see Figure 7 (c) and (d), noting the change of scale with respect to (a) and (b)).

A method is devised below that permits us to isolate the time-evolving synergistic effects produced by the *Mean* state and the three PV anomalies on the surface-height tendency and vertical motion around the storm. This method is based on a combination of a PV-based prognostic system (Section 4.1) and a factor-separation technique (Section 4.2).

4.1. PV-based prognostic system

A set of prognostic balance equations can be derived from the PV diagnostic system presented in Section3.1. Equivalent equations for geographical (lon, lat) coordinates can be found in Davis and Emanuel (1991, appendix B). We start by obtaining tendency equations for (ϕ^t, ψ^t) by taking the local time derivatives of Charney's (1955) nonlinear balance equation (4) and the approximate form of Ertel PV (5):

$$\nabla^2\phi^t = \nabla\cdot f\nabla\psi^t + 2m^2\left(\frac{\partial^2\psi^t}{\partial x^2}\frac{\partial^2\psi}{\partial y^2} + \frac{\partial^2\psi}{\partial x^2}\frac{\partial^2\psi^t}{\partial y^2} - 2\frac{\partial^2\psi}{\partial x\partial y}\frac{\partial^2\psi^t}{\partial x\partial y}\right) \tag{10}$$

and

$$q^t = \frac{g\kappa\pi}{p}\left\{(f + m^2\nabla^2\psi)\frac{\partial^2\phi^t}{\partial\pi^2} + m^2\frac{\partial^2\phi}{\partial\pi^2}\nabla^2\psi^t - m^2\left(\frac{\partial^2\psi^t}{\partial x\partial\pi}\frac{\partial^2\phi}{\partial x\partial\pi} + \frac{\partial^2\psi}{\partial x\partial\pi}\frac{\partial^2\phi^t}{\partial x\partial\pi} + \frac{\partial^2\psi^t}{\partial y\partial\pi}\frac{\partial^2\phi}{\partial y\partial\pi} + \frac{\partial^2\psi}{\partial y\partial\pi}\frac{\partial^2\phi^t}{\partial y\partial\pi}\right)\right\}. \tag{11}$$

Recalling that ϕ and ψ are known aspects of the circulation after the inversion of q through Equations (4) and (5), Equations (10) and (11) can be solved for the geopotential and stream-function tendencies, provided q^t is known. This can be calculated using the following form of the Ertel PV tendency equation:

$$q^t = -m(\mathbf{V}_\psi + \mathbf{V}_\chi)\cdot\nabla q - \omega^*\frac{\partial q}{\partial\pi} + \frac{m}{\rho}\boldsymbol{\eta}\cdot\nabla LH, \tag{12}$$

where the vertical velocity $\omega^* \equiv \mathrm{d}\pi/\mathrm{d}t$ and irrotational wind $\mathbf{V}_\chi$ must be formally retained (Krishnamurti, 1968; Iversen and Nordeng, 1984), meaning that we cannot simply advect q with the non-divergent wind $\mathbf{V}_\psi$. The horizontal winds are given by the familiar expressions

DOI: 10.1002/qj

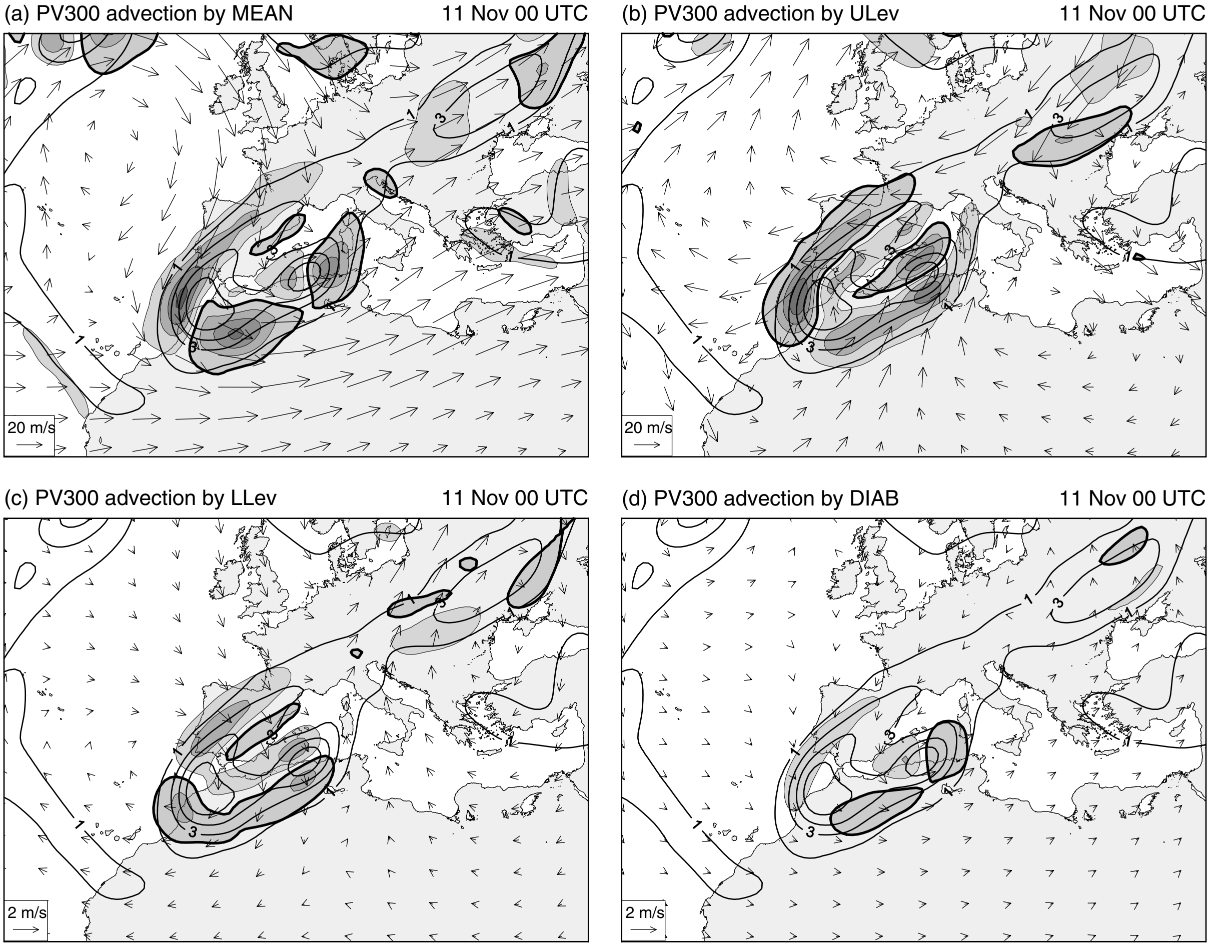

Figure 7. PV advection at 300 hPa at 00 UTC on 11 November, produced by: (a) the *Mean* flow; (b) the *ULev*-inverted flow; (c) the *LLev*-inverted flow; (d) the *Diab*-inverted flow. The advection field is shown as shaded for negative PV advection, and shaded within thick-line-highlighted regions for positive PV advection, starting at −2 PVU/12 h and 2 PVU/12 h respectively, with a contour interval of 5 PVU/12 h in panels (a) and (b) and starting at −0.2 PVU/12 h and 0.2 PVU/12 h with a contour interval of 0.5 PVU/12 h in panels (c) and (d). The PV field and the PV-inverted advective flow at 300 hPa are also shown using continuous lines (in PVU) and wind vectors (see reference vector at the bottom-left of each panel).

$\mathbf{V}_\psi = m\mathbf{k} \times \nabla\psi$ and $\mathbf{V}_\chi = m\nabla\chi$, and ω^* is related to the more traditional vertical velocity ω in pressure coordinates through the formula $\omega^* = (\kappa\pi/p)\omega$. The only non-conservative effect that is included in this equation is the latent-heat release $LH \equiv \mathrm{d}\theta/\mathrm{d}t$ from non-convective clouds where the air is ascending on a broad scale. This diabatic term is parametrized in terms of ω^* as explained in Davis and Emanuel (1991).

The prognostic system is closed by means of an omega equation for ω^* and the continuity equation for the velocity potential χ, which in this context take the following forms:

$$\begin{aligned} &f\eta\frac{\partial}{\partial\pi}\left\{\pi^{1-1/\kappa}\frac{\partial}{\partial\pi}(\pi^{1/\kappa-1}\omega^*)\right\} + m^2\nabla^2\left(\frac{\partial^2\phi}{\partial\pi^2}\omega^*\right) \\ &- m^2 f\frac{\partial}{\partial\pi}\left(\frac{\partial\omega^*}{\partial x}\frac{\partial\psi}{\partial x\partial\pi} + \frac{\partial\omega^*}{\partial y}\frac{\partial\psi}{\partial y\partial\pi}\right) \\ &+ \left(f\frac{\partial\eta}{\partial\pi}\frac{1/\kappa-1}{\pi} - f\frac{\partial^2\eta}{\partial\pi^2}\right)\omega^* \\ &= m^3\nabla^2\left\{(\mathbf{V}_\psi + \mathbf{V}_\chi)\cdot\nabla\theta\right\} \\ &+ mf\frac{\partial}{\partial\pi}\left\{(\mathbf{V}_\psi + \mathbf{V}_\chi)\cdot\nabla\eta\right\} - m^2\nabla f\cdot\nabla\frac{\partial\psi^t}{\partial\pi} \\ &- 2m^4\frac{\partial}{\partial\pi}\left(\frac{\partial^2\psi^t}{\partial x^2}\frac{\partial^2\psi}{\partial y^2} + \frac{\partial^2\psi}{\partial x^2}\frac{\partial^2\psi^t}{\partial y^2}\right. \\ &\left. - 2\frac{\partial^2\psi}{\partial x\partial y}\frac{\partial^2\psi^t}{\partial x\partial y}\right) - m^2\nabla^2(LH), \end{aligned} \tag{13}$$

and

$$m^2\nabla^2\chi + \pi^{1-1/\kappa}\frac{\partial}{\partial\pi}(\pi^{1/\kappa-1}\omega^*) = 0. \tag{14}$$

The complete system of equations (10)–(14), formulated in finite differences with vertical staggering of the ω^* levels, is solved iteratively by a simultaneous relaxation method for the fields ϕ^t, ψ^t, q^t, ω^* and χ. It is important to note that the equations are not integrated in time, but simply solved for the instantaneous tendencies. Homogeneous lateral boundary conditions are applied on

DOI: 10.1002/qj

a large-enough domain for each field ($\phi^t = \psi^t = q^t = \omega^* = \chi = 0$), while at the top and bottom boundaries more complex conditions are used: the vertical velocities are zero and topographic respectively; and Neumann-type definitions are used for the tendencies ϕ^t and ψ^t:

$$\frac{\partial \phi^t}{\partial \pi} = f\frac{\partial \psi^t}{\partial \pi} = -\theta^t, \tag{15}$$

where the necessary potential-temperature tendencies at both levels are evaluated from the thermodynamic equation:

$$\theta^t = -m(\mathbf{V}_\psi + \mathbf{V}_\chi)\cdot\nabla\theta - \omega^*\frac{\partial\theta}{\partial\pi} + LH. \tag{16}$$

4.2. Application of factor separation

The prognostic system described above is solved at 00 and 12 UTC during the life cycle of the Mediterranean cyclone, that is, from 00 UTC on 10 November to 12 UTC on 12 November, as was done for Figure 5. Of particular interest for describing the cyclogenesis process are the calculated fields of surface height tendency and vertical motion around the storm. Examples of these outputs are plotted as unshaded line contours in Figures 9–10 and 11–12 respectively, for 11 November at 00 UTC (the time of the storm's peak intensity). As expected, the results identify the strong cyclogenesis and upward motion plume over the western Mediterranean basin at that time (recall Figures 1 and 2). Since these results emerge from the total balance flow, described by q, ϕ and ψ, we may refer to their signatures in Figures 9–10 and 11–12 as the *total* fields for the surface height tendency and vertical motion.

In the present context, we are seeking a way to split the total fields into the *contributions* from the four constituent PV elements of q (i.e. the basic state *Mean* plus the three anomalies *ULev*, *LLev* and *Diab*), including all their possible interactions. This appears to be a feasible task given the definitions (3) and (7) and our ability to repeat the above calculations after subtracting from the input (q, ϕ, ψ) fields one or several PV anomalies. This is, in essence, a factor-separation exercise, as is commonly applied to computer-based numerical representations of weather events, except that we are not dealing with numerical simulations progressing in time but with instantaneous solutions to the PV-based prognostic system of equations. Of particular interest here is the factor-separation technique of Stein and Alpert (1993), which was designed to account explicitly for the synergistic effects besides the individual contributions of a given set of factors. The basic idea of this technique is illustrated in Figure 8 for the present case of three factors: any total field (e.g. the surface-height tendency on 11 November at 00 UTC – rectangle in the figure) will consist of a contribution from the *Mean* flow, independent of the three PV anomalies (region E_0 in the figure), plus the mutually-independent contributions from the anomalies (regions E_1, E_2 and E_3) and the double or triple interactions between the factors (E_{12}, E_{13}, E_{23} and E_{123}). We could refer to these three families as the basic, individual and synergistic effects, respectively, although it must be noted that E_1, E_2 and E_3 depend on synergies with the basic *Mean* flow, since this is a fundamental aspect of the total circulation. For instance, E_1 would include, among other actions, the effects on the surface height tendency due to the advection of the *ULev* PV anomaly by the basic flow; E_{12} would include, among other processes, the forcing associated with the low-level thermal advection of *LLev* motivated by the simultaneous presence of *ULev* and its circulation; and so on.

By switching on and off different combinations of the PV anomalies in the (q, ϕ, ψ) flow state, we can include or exclude different subsets of the effects displayed in Figure 8 from the corresponding solution to the PV-based prognostic system. This means that, with the proper number of flow states, all the individual and synergistic effects can be isolated. Stein and Alpert (1993) show that the complete separation of n factors requires 2^n experiments. Accordingly, eight distinct flow configurations are necessary in this study (see Table II). The complete set of effects can be isolated through the algebraic combination of the corresponding solutions:

- $E_0 = F_0$;
- $E_1 = F_1 - F_0$;
- $E_2 = F_2 - F_0$;
- $E_3 = F_3 - F_0$;
- $E_{12} = F_{12} - (F_1 + F_2) + F_0$;
- $E_{13} = F_{13} - (F_1 + F_3) + F_0$;
- $E_{23} = F_{23} - (F_2 + F_3) + F_0$;
- $E_{123} = F_{123} - (F_{12} + F_{13} + F_{23}) + (F_1 + F_2 + F_3) - F_0$.

Here, a more intuitive notation is adopted for these effects, by using the terms *Mean*, *ULev*, *LLev*, *Diab*, *ULev/LLev*, *ULev/Diab*, *LLev/Diab* and *ULev/LLev/Diab*, respectively.

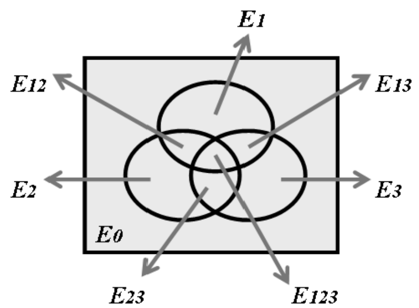

Figure 8. Schematic diagram showing the effects on a total field (rectangle) due to the *Mean* flow (E_0) and caused by the individual and synergistic actions of the three factors under study – (1) *ULev*, (2) *LLev* and (3) *Diab*. These effects are isolated by the factor-separation technique (see text).

DOI: 10.1002/qj

Table II. The eight different atmospheric-flow states calculated using the PV-based prognostic system. The results are combined in the factor-separation method (see text).

Flow state	(0) *Mean*	(1) *ULev*	(2) *LLev*	(3) *Diab*
F_0	yes	no	no	no
F_1	yes	yes	no	no
F_2	yes	no	yes	no
F_3	yes	no	no	yes
F_{12}	yes	yes	yes	no
F_{13}	yes	yes	no	yes
F_{23}	yes	no	yes	yes
F_{123}	yes	yes	yes	yes

4.3. Results of the dynamic approach

The above method has been applied to isolate the impacts and interactions of the PV anomalies on the surface height tendency and vertical-motion fields responsible for driving the November 2001 cyclonic disturbance. The results are plotted for the mature storm in Figures 9–12, as spatial patterns with positive and negative signals of the eight different contributions to the total fields (these are also included in the figures for reference). Particular attention is paid to signatures of negative height tendency and positive vertical velocity occurring over the western Mediterranean region, thus contributing to the cyclogenesis mechanism.

The action of the background flow *Mean* is to help propagate the surface cyclone eastwards along the Mediterranean waters (Figure 9(a)). Since the *Mean* PV distribution, as defined, is an invariant aspect of the time-evolving circulation, exactly the same pattern is found for its contribution during the development and decay phases of the baroclinic system (not shown). With regard to the vertical velocity, *Mean* exerts only a very minor influence over the area of interest (Figure 11(a)).

The individual effect of *ULev* is crucial for the cyclogenesis (Figure 9(b)). It is responsible for a significant fraction of the surface-pressure fall calculated over the western Mediterranean. Its influence is also notable in North Africa during the development phase of the cyclone (Figure 13(a)), and around the southern coast of France during its last phase (Figure 14(a)). Such spatial evolution of the *ULev* forcing, from south to north, is fully

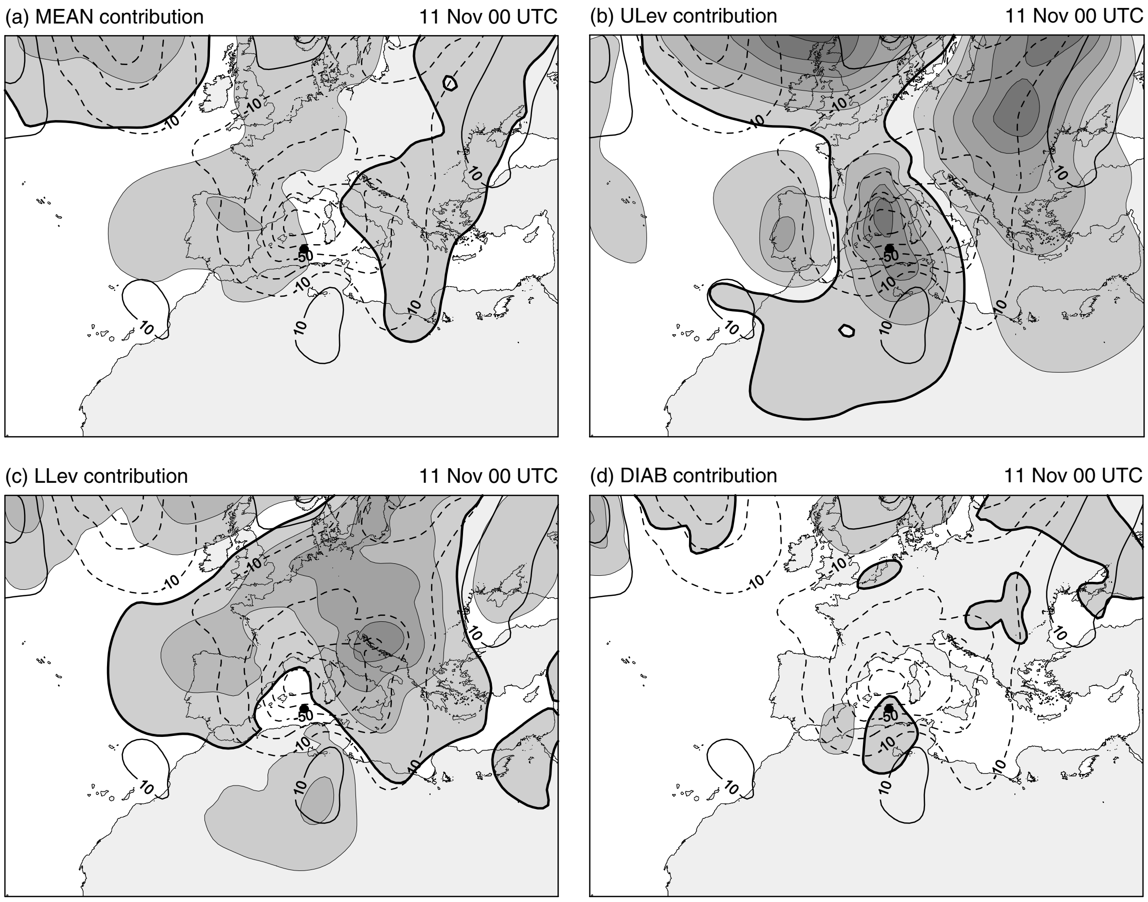

Figure 9. Factor-separation results on the geopotential-height tendency at 925 hPa, corresponding to the mature phase of the cyclone (11 November at 00 UTC). The contributions from (a) *Mean*, (b) *ULev*, (c) *LLev* and (d) *Diab* are shown as shaded for positive height tendency, and shaded within thick-line-highlighted regions for negative height tendency, starting at −5 gpm/12 h and 5 gpm/12 h respectively, with a contour interval of 10 gpm/12 h. The total height-tendency field at 925 hPa is also shown, with dashed lines representing negative values starting at −10 gpm/12 h and continuous lines representing positive values starting at 10 gpm/12 h, with a contour interval of 20 gpm/12 h. The black circle located in the southern Mediterranean indicates the central position of the cyclone (see Figure 1(d)).

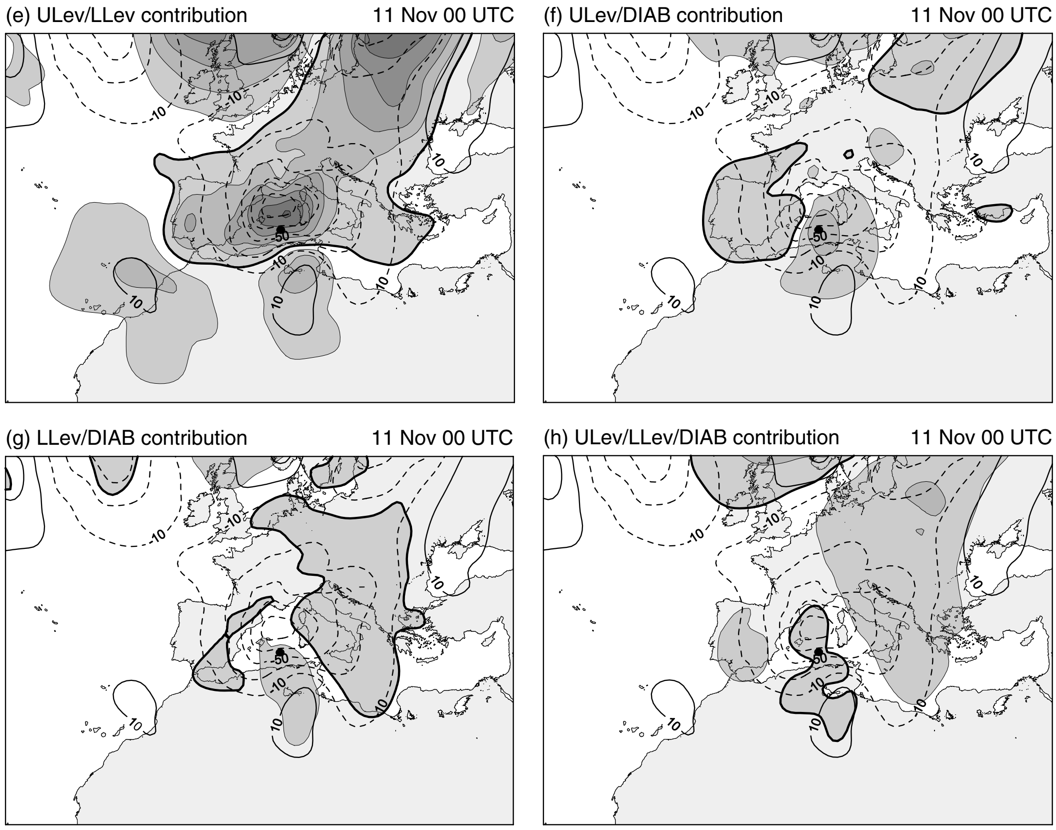

Figure 10. As Figure 9, but showing the contributions from (e) *ULev/LLev*, (f) *ULev/Diab*, (g) *LLev/Diab* and (h) *ULev/LLev/Diab*.

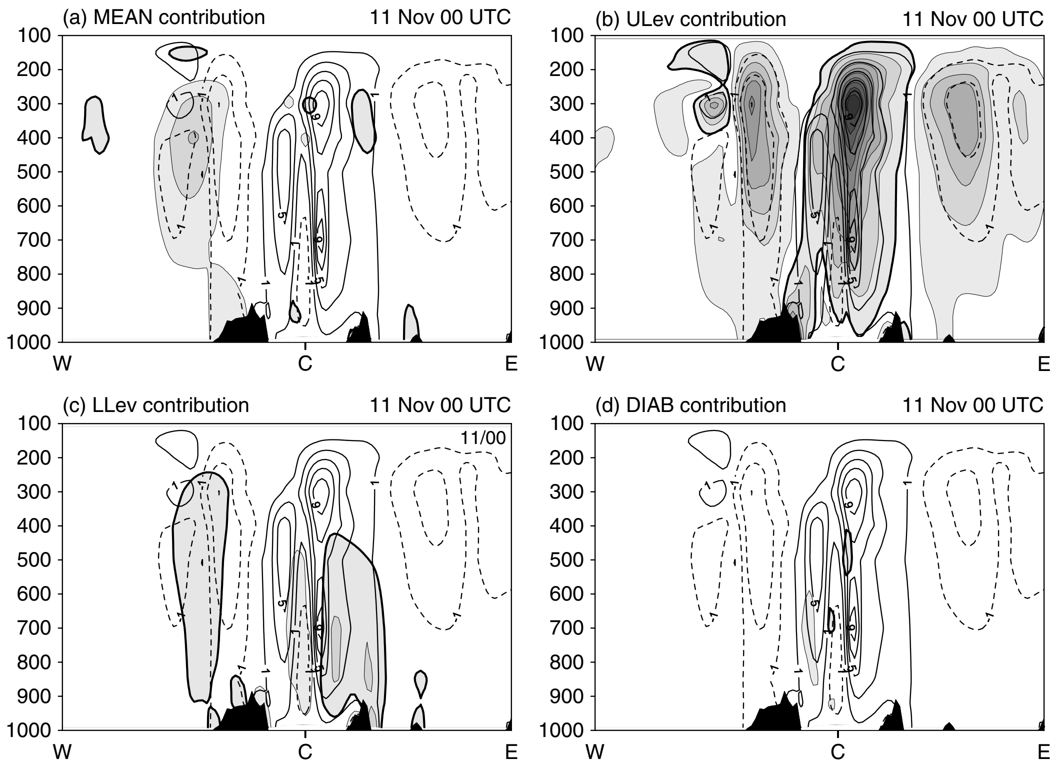

Figure 11. Factor-separation results on the vertical velocity in the west–east vertical cross section shown in Figure 3(b), corresponding to the mature phase of the cyclone (11 November at 00 UTC). The contributions from (a) *Mean*, (b) *ULev*, (c) *LLev* and (d) *Diab* are shown as shaded for downward motion, and shaded within thick-line-highlighted regions for upward motion, starting at −0.5 cm/s and 0.5 cm/s respectively, with a contour interval of 1 cm/s. The total vertical-velocity field is also shown, with dashed lines representing negative values starting at −1 cm/s and continuous lines representing positive values starting at 1 cm/s, with a contour interval of 2 cm/s. The letter C at the bottom of the panels indicates the position of the cyclone.

DOI: 10.1002/qj

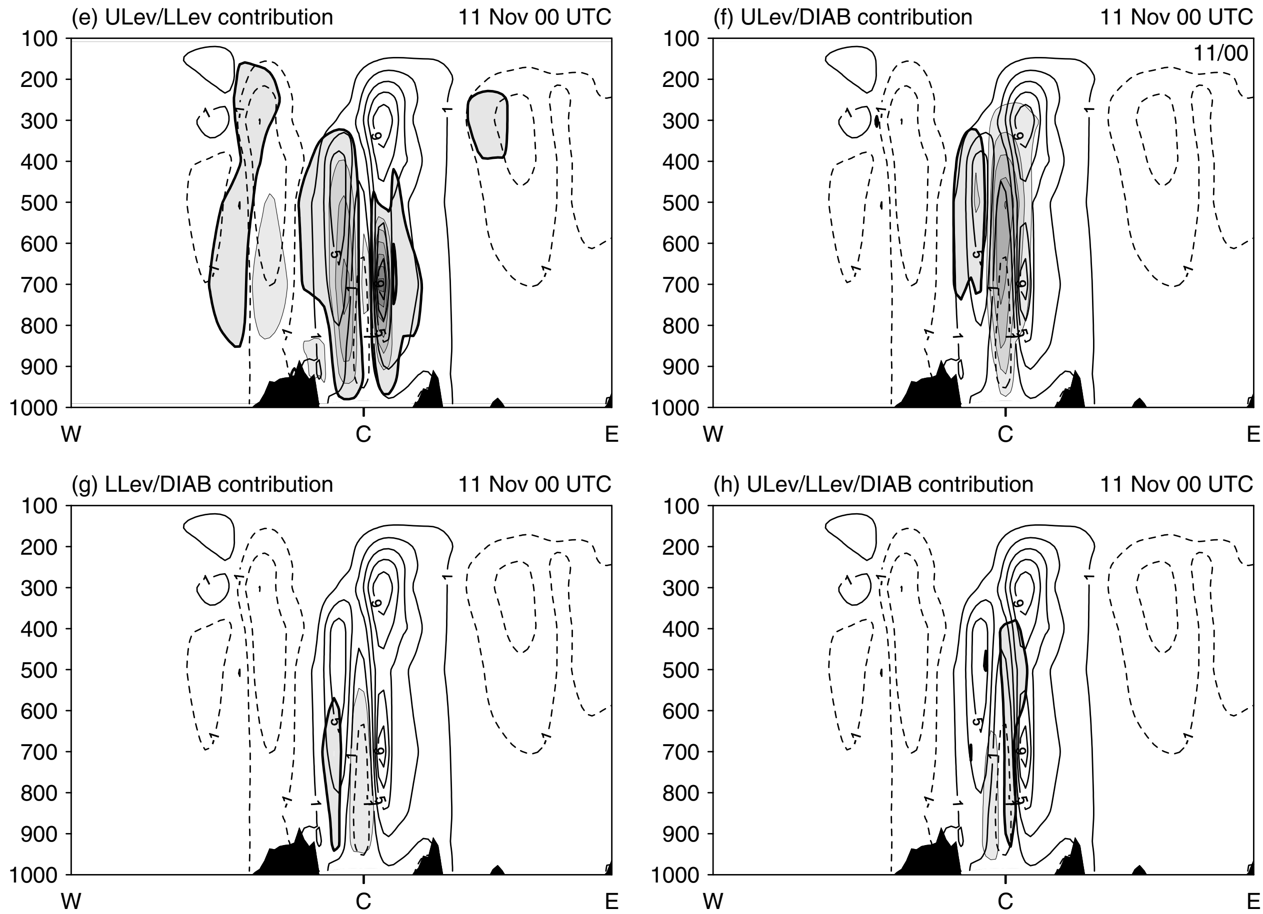

Figure 12. As Figure 11, but showing the contributions from (e) *ULev*/*LLev*, (f) *ULev*/*Diab*, (g) *LLev*/*Diab* and (h) *ULev*/*LLev*/*Diab*.

consistent with the evolution of the corresponding upper-level PV anomaly over the period, especially of its eastern lobe (Figure 3). Recall from Figure 7 that the upper-level PV advection is dominated by the *Mean* and *ULev* winds; both are explicitly included in the factor separation of *ULev*. On the other hand, the *ULev* factor is largely responsible for the wavy pattern in the total vertical motion diagnosed across the domain (see Figure 11(b)). Clearly, the factor-separation results confirm not only the precursor characteristics of the upper-level trough for the development of the cyclone, but also its active involvement during the later phases of the system, irrespective of its interaction with the low-level baroclinicity.

Individually, *LLev* also represents a significant contribution to the cyclone's growth, movement and decay. During the mature phase, its main action is concentrated along the northern flank of the cyclone (Figure 9(c)), that is, in the zones affected by well-defined surface fronts and where the warm advection is most clear (recall Figure 6(c)). Thus the pattern of the *LLev* contribution favours the northeastward propagation of the surface disturbance that was observed in Figure 1. A similar effect, though with lower magnitude, is calculated for 12 November (Figure 14(b)), whereas at the early stages of the system *LLev* is basically contributing to its growth (Figure 13(b)). Regarding the upward-motion forcing over the western Mediterranean, the main signature associated with *LLev* is found again along the eastern flank of the cyclone (Figure 11(c)), that is, in the area of enhanced low-level warm advection.

The very localized nature of the *Diab* PV anomaly (Figure 3) implies a comparatively weak individual effect on both the surface height tendency and the vertical motion (Figures 9(d) and 11(d) respectively). This effect is essentially linked to the PV advection induced by the background flow, and therefore has a dipolar structure about the Algerian coast surrounding the anomaly. A similar weak effect is found during the development and decay phases of the baroclinic system (not shown).

The *ULev*/*LLev* interaction is a leading agent for generating and driving the November 2001 cyclone (Figure 10(e)), in agreement with the conceptual model of baroclinic developments formulated by 'PV thinking'. On the surface height tendency, this factor attains a magnitude comparable to or even higher than the above-mentioned individual contribution of *ULev* (compare with Figure 9(b)), with the particularity that the pattern over the western Mediterranean very much resembles the total tendency field. The importance of the synergistic action is well understood if one remembers the appreciable warm-advection values that are induced at low levels (recall Figure 6(b)). The role of this factor

DOI: 10.1002/qj

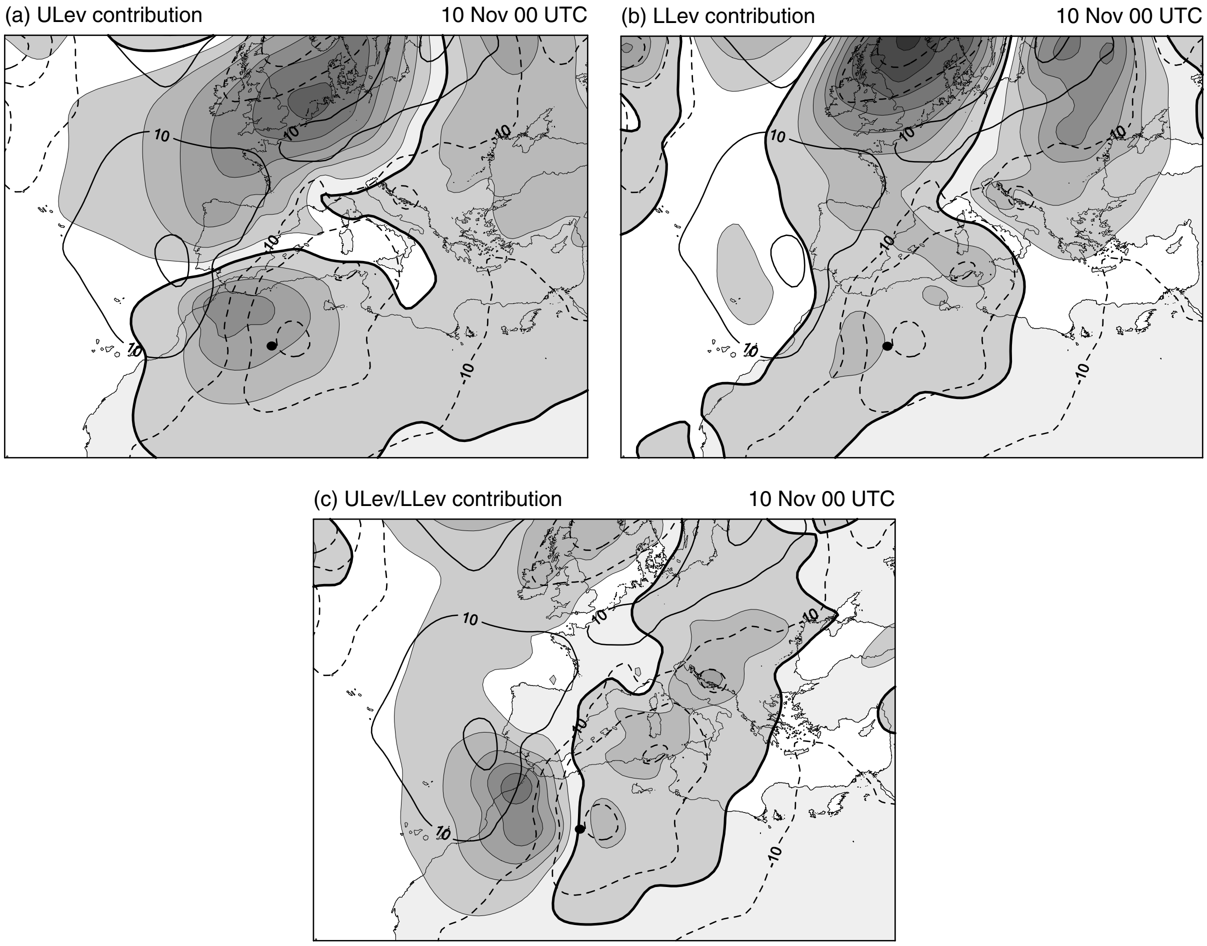

Figure 13. As Figure 9, but for the development phase of the cyclone (10 November at 00 UTC, see Figure 1(b)); contributions from (a) *ULev*, (b) *LLev* and (c) *ULev*/*LLev*.

is also noted on the vertical-motion field (Figure 12(e)), helping to explain a significant fraction of the Mediterranean upward-motion plumes. It is worth remarking that, in contrast with the *ULev* effect (Figure 11(b)), in this case the contribution to the vertical velocity is focused at lower-to-mid-tropospheric levels, because of the different nature of the two mechanisms (upper-level PV advection in *ULev* and vertical interaction through the thermal advection in *ULev*/*LLev*). The *ULev*/*LLev* coupling is also very effective over North Africa and the Mediterranean Sea during the genesis of the disturbance (Figure 13(c)), but the positive height-tendency signal obtained over the northwestern coast of Africa – a consequence of the intense cold advection occurring west of the cyclone – is remarkable (compare with Figure 1(b)). The transition of the circulation system towards less negative vertical tilting and diminished temperature gradients after its mature stage (Figure 1) implies increasingly weak thermal-advection values and, correspondingly, only minor cooperation between *ULev* and *LLev* in support of the cyclone at the end of the period (Figure 14(c)).

The *ULev*/*Diab* effect on the surface height tendency is most relevant during the mature phase of the disturbance (Figure 10(f)). It has a dipolar structure like the one noted for *Diab* (Figure 9(d)), but of larger magnitude and reversed sign. The sign reversal is due to the opposite directions of the *Mean* and *ULev* advective winds acting on the *Diab* PV anomaly (compare the wind fields between panels (a) and (b) in Figures 6 and 7). Overall, the *ULev*/*Diab* factor contributes to cyclogenesis only to the west of the cyclone; over and to the east of the cyclone its effect is essentially cyclolytic (Figure 10(f)). The contribution of this factor to the vertical-motion field attains moderate values at mid-tropospheric levels over the Mediterranean Sea, with a spatial pattern similar to the total field (Figure 12(f)).

The *LLev*/*Diab* synergism is also cyclolytic over the mature cyclone (Figure 10(g)), and its contribution to the vertical-motion field in the analysed cross section is rather low (Figure 12(g)). As for the last factor, its influence during the development and decay phases of the system is quite low (not shown). Since the *LLev*/*Diab* mechanism incorporates the effects of the *Diab* PV advection by the *LLev*-induced flow and the *LLev* thermal advection by the *Diab*-induced flow, which are of comparable magnitude, the precise interpretation of the *LLev*/*Diab* spatial pattern displayed on Figure 10(g) appears to be more intricate than for the other factors.

Finally, we can analyse the contribution of the triple interaction *ULev*/*LLev*/*Diab* (Figures 10(h) and 12(h)).

DOI: 10.1002/qj

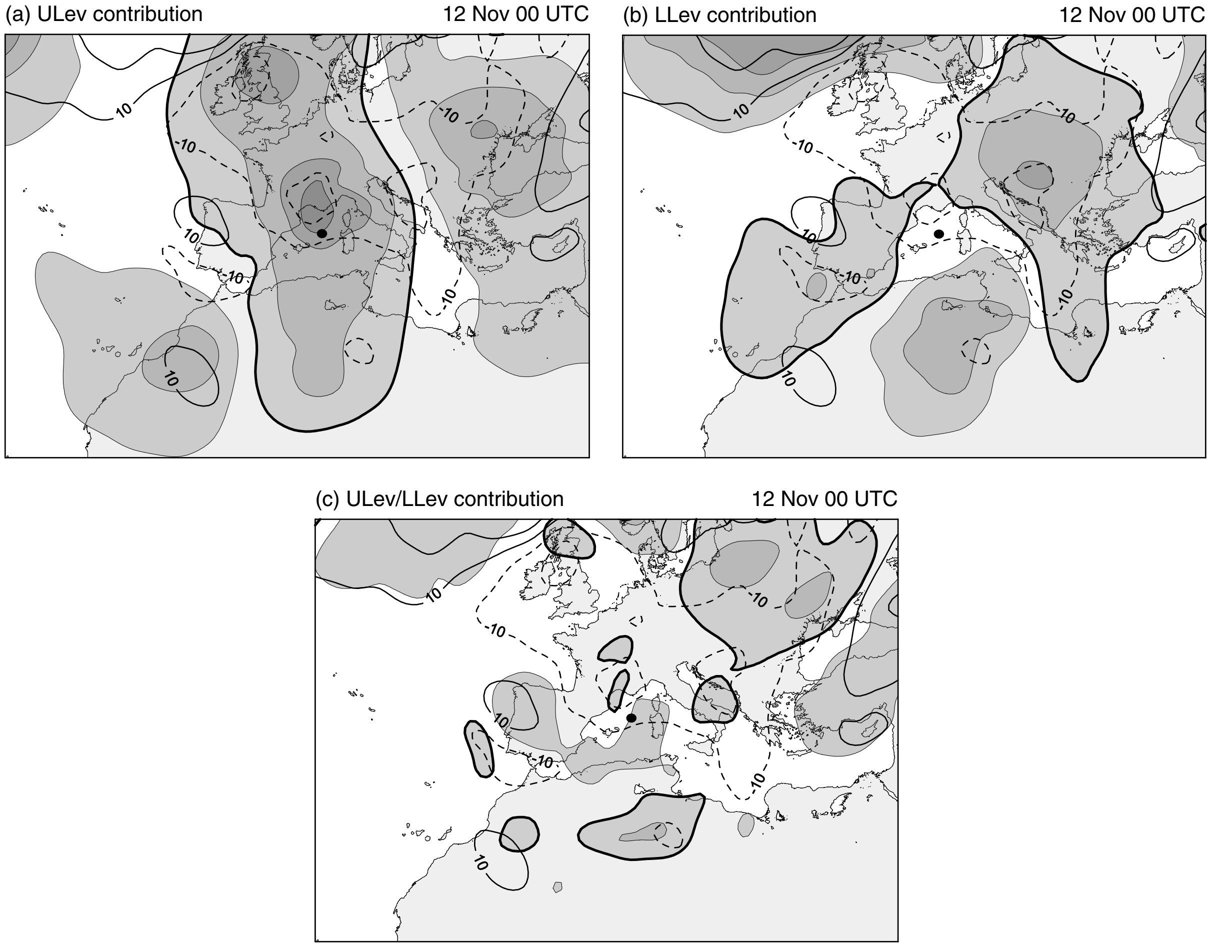

Figure 14. As Figure 9, but for the decay phase of the cyclone (12 November at 00 UTC, see Figure 1(f)); contributions from (a) *ULev*, (b) *LLev* and (c) *ULev/LLev*.

Because of the involvement of the small *Diab* PV anomaly in this factor, it exerts only a secondary role, like *Diab*, *ULev/Diab* and *LLev/Diab*. Interestingly, the obtained height-tendency pattern almost perfectly balances the *LLev/Diab* contribution (compare with Figure 10(g)), helping the deepening of the cyclone in this case. It is quite difficult to give a plausible physical explanation for the *ULev/LLev/Diab* effect; this is a well-known handicap of the Stein–Alpert factor-separation technique when more than two factors are studied.

In summary, it can be concluded that the most intense phase of the November 2001 Mediterranean cyclone was regulated by the *Mean*, *ULev*, *LLev* and *ULev/LLev* processes: *Mean* and *LLev* assisted in the northeastward propagation of the disturbance, and to some extent in its intensification (especially *LLev* during its African phase); both *ULev* and *ULev/LLev* were fundamental for the African cyclogenesis and further intensification of the disturbance over the western Mediterranean, although *ULev/LLev* quickly decayed after the cyclone's maturation. The remaining mechanisms (*Diab*, *ULev/Diab*, *LLev/Diab* and *ULev/LLev/Diab*) were most relevant during the mature phase of the system, but, compared to the first group, they only exerted a secondary role, because of the limited strength and spatial dimensions of the *Diab* PV anomaly. According to the factor-separation results, the development and mature phases of the baroclinic disturbance can be described as a meteorological scenario of effective cooperation among the background flow and the PV anomalies over the surface cyclone domain (Figures 13, 9 and 10), whereas the decay of the system is linked to a scenario of much weaker, or even cyclolytic, interactions between some of these factors (Figure 14).

5. Summary and discussion

An increasing number of researchers in theoretical and applied dynamic meteorology use time-evolving PV maps for their analyses and inferences, often as a modern complement to more classical approaches (such as QG diagnosis). In particular, the so-called 'PV thinking' that emerges from the invertibility and conservation principles has produced notable advances in understanding the processes involved in the mechanics of extratropical cyclones.

In this work, I have tried to emphasize the additional value of quantitative versus qualitative approaches, and dynamic versus static approaches. To that end, the combination of a PV-based prognostic system of closed equations and a factor-separation technique has been proposed. Its implementation provides an efficient and computationally-cheap algorithm that allows us to isolate the individual and synergistic effects of a given set of PV anomalies on the cyclone's growth, trajectory, structure and decay. The potentialities of this method have been illustrated for the western Mediterranean cyclone of 10–12 November 2001, the worst storm to affect the Balearic Islands in recent decades. The case study was aimed at isolating the effects of the background flow and the PV anomalies linked to the undulating tropopause, low-level baroclinicity and condensational latent-heat release. Vertical velocity and low-level height tendency around the storm domain have been examined at various time intervals during its life cycle. The obtained results are in good agreement with the general hypotheses of the conceptual model of mid-latitude baroclinic developments, although with unprecedented quantitative detail with regard to the specific partition of the effects among the diverse lateral and vertical interactions of the PV anomalies.

However, the method has some drawbacks, relating to the subjective choice of the PV anomalies. First of all, the selection of a background state from which to define a perturbation PV field is arbitrary: a low-pass-filtered flow state, the temporal or spatial average over a certain window, the region's climatology, or even an analytical model, would all be acceptable choices. The way in which the perturbation field is broken into different PV elements is also subjective, dictated by the specific interests of the researcher. In this regard, our general recommendation would be to consider a reduced number of dynamically-meaningful anomalies, as was done for the 10–12 November 2001 case study. Finally, physical interpretation of some calculated synergies might become problematic, depending on the number of selected PV anomalies. Although the method can isolate any combined effect, regardless of its complexity, it would be virtually impossible to visualize, in terms of the most fundamental forcing mechanisms (i.e. temperature and vorticity advections), triple, quadruple or higher-order PV interactions.

In spite of these issues, it would be a worthwhile exercise to exploit this novel technique in a systematic intercomparison of a large collection of cyclonic events, using the same definitions for the background-flow and PV anomalies: that is, a PV-based categorization of cyclones according to the impacts and interactions of the anomalies during the life cycle of the storm, from its genesis to its decay. A task like this appears to be especially promising in the Mediterranean geographical domain, where cyclones with very diverse influences develop, thanks to the special characteristics of the basin: it is located in the extratropics and therefore becomes episodically affected by mid-latitude upper-level-jet and frontal activity; its prominent orography favours lee cyclogenesis, with some of the initially-shallow disturbances undergoing baroclinic growth; the warm sea can act as an important local source of sensible and latent heat for the storms; and the arid, elevated surface of the southernmost landmasses, like Iberia and the North African plateau, provides a significant heat input to the overlying air, which, when advected to contiguous regions, will alter the static stability and mechanisms of frontogenesis and frontolysis. Since our method admits, as additional factors, the orographic forcing and diabatic contribution (recall the topographic boundary condition and *LH* term respectively in the formulae of Section 4), both of which are easy to switch on and off in the applied separation technique, all the above influences could potentially be investigated and incorporated in such a projected climatology of Mediterranean cyclones.

Acknowledgements

The development of this study was made with support from the Spanish Ministry of Education and Science, research project CGL 2005-03918/CLI (PRECIOSO). The author also acknowledges earlier computer support provided by NCAR Scientific Computer Division (sponsored by the US National Science Foundation), which permitted access to the NCEP grid meteorological analyses.

References

Ahmadi-Givi F, Craig GC, Plant RS. 2004. The dynamics of a midlatitude cyclone with very strong latent-heat release. *Q. J. R. Meteorol. Soc.* **130**: 295–323.

Bluestein HB. 1993. *Synoptic-Dynamic Meteorology in Midlatitudes*, vol. 2. Oxford University Press: 594 pp.

Bolin B. 1955. Numerical forecasting with the barotropic model. *Tellus* **7**: 27–49.

Charney JG. 1947. The dynamics of long waves in a baroclinic westerly current. *J. Meteorol.* **4**: 135–163.

Charney JG. 1955. The use of primitive equations of motion in numerical prediction. *Tellus* **7**: 22–26.

Clough SA, Davitt CSA, Thorpe AJ. 1996. Attribution concepts applied to the omega equation. *Q. J. R. Meteorol. Soc.* **109**: 565–573.

Conte M. 1986. The meteorological bomb in the Mediterranean: a synoptic climatology. WMO/TD 128, App. 4, pp 17–31.

Davis CA. 1992a. A potential-vorticity diagnosis of the importance of initial structure and condensational heating in observed extratropical cyclogenesis. *Mon. Weather Rev.* **120**: 2409–2428.

Davis CA. 1992b. Piecewise potential vorticity inversion. *J. Atmos. Sci.* **49**: 1397–1411.

Davis CA, Emanuel KA. 1991. Potential vorticity diagnostics of cyclogenesis. *Mon. Weather Rev.* **119**: 1929–1953.

Eady TE. 1949. Long waves and cyclone waves. *Tellus* **1**: 33–52.

Ertel H. 1942. Ein neuer hydrodynamischer wirbelsatz. *Meteorol. Z.* **59**: 271–281.

Genovés A, Jansá A. 1991. 'The use of potential vorticity maps in monitoring shallow and deep cyclogenesis in the Western Mediterranean'. WMO/TD 420, pp 55–65.

Hakim GH, Keyser D, Bosart LF. 1996. The Ohio valley wave-merger cyclogenesis event of 25–26 January 1978. Part II: Diagnosis using quasigeostrophic potential vorticity inversion. *Mon. Weather Rev.* **124**: 2176–2205.

Homar V, Ramis C, Alonso S. 2000. A deep cyclone of African origin over the western Mediterranean: diagnosis and numerical simulation. *Ann. Geophys.* **20**: 93–106.

Hoskins BJ, McIntyre ME, Robertson AW. 1985. On the use and significance of isentropic potential vorticity maps. *Q. J. R. Meteorol. Soc.* **111**: 877–946.

Huo Z, Zhang DL, Gyakum JR. 1998. An application of potential vorticity inversion to improving the numerical prediction of the March 1993 superstorm. *Mon. Weather Rev.* **126**: 424–436.

DOI: 10.1002/qj

Huo Z, Zhang DL, Gyakum JR. 1999a. Interaction of potential vorticity anomalies in extratropical cyclogenesis. Part I: Static piecewise inversion. *Mon. Weather Rev.* **127**: 2546–2561.

Huo Z, Zhang DL, Gyakum JR. 1999b. Interaction of potential vorticity anomalies in extratropical cyclogenesis. Part II: Sensitivity to initial perturbations. *Mon. Weather Rev.* **127**: 2563–2575.

Iversen T, Nordeng TE. 1984. A hierarchy of nonlinear filtered models – numerical solutions. *Mon. Weather Rev.* **112**: 2048–2059.

Jansá A, Romero R (eds). 2003. *Mediterranean Storms: 4th Plinius Conference 2002 (CD Proceedings)*. ISBN 84-7632-792-7. Universitat de les Illes Balears: 07 122 Palma de Mallorca, Spain.

Jansá A, Genovés A, Picornell MA, Campins J, Riosalido R, Carretero O. 2001. Western Mediterranean cyclones and heavy rain. Part II: Statistical approach. *Meteorol. Appl.* **8**: 43–56.

Krishnamurti TN. 1968. A diagnostic balanced model for studies of weather systems of low and high latitudes, Rossby number less than 1. *Mon. Weather Rev.* **96**: 197–207.

Martín A, Romero R, Homar V, Luque A, Alonso S, Rigo T, Llasat MC. 2007. Sensitivities of a flash flood event over Catalonia: A numerical analysis. *Mon. Weather Rev.* **135**: 651–669.

Pettersen S. 1956. *Weather Analysis and Forecasting*. McGraw-Hill: New York.

Pettersen S, Smebye SJ. 1971. On the development of extratropical cyclones. *Q. J. R. Meteorol. Soc.* **97**: 457–482.

Radinovic D. 1987. 'Mediterranean cyclones and their influence on the weather and climate'. PSMP Rep. Ser. 24. WMO.

Reiter E. 1975. *Handbook for Forecasters in the Mediterranean. Part 1: General Description of the Meteorological Processes*. Naval Environmental Research Facility: Monterey, California.

Romero R. 2001. Sensitivity of a heavy rain producing Western Mediterranean cyclone to embedded potential vorticity anomalies. *Q. J. R. Meteorol. Soc.* **127**: 2559–2597.

Rossby CG. 1940. Planetary flow patterns in the atmosphere. *Q. J. R. Meteorol. Soc.* **66**: 68–87 (supplement).

Sanders F. 1986. Explosive cyclogenesis over the west central North Atlantic Ocean 1981–1984. Part I: Composite structure and mean behavior. *Mon. Weather Rev.* **114**: 1781–1794.

Sanders F. 1988. Life history of mobile troughs in the upper westerlies. *Mon. Weather Rev.* **118**: 2629–2648.

Speranza A, Buzzi A, Trevisan A, Malguzzi P. 1985. A theory of deep cyclogenesis in the lee of the Alps. Part 1: modifications of baroclinic instability by localized topography. *J. Atmos. Sci.* **42**: 1521–1535.

Stein U, Alpert P. 1993. Factor separation in numerical simulations. *J. Atmos. Sci.* **50**: 2107–2115.

Thorpe AJ. 1985. Diagnosis of balanced vortex structure using potential vorticity. *J. Atmos. Sci.* **42**: 397–406.

Thorpe AJ. 1997. Attribution and its application to mesoscale structure associated with tropopause folds. *Q. J. R. Meteorol. Soc.* **123**: 2377–2399.

Ziemianski MZ, Thorpe AJ. 2000. The dynamical consequences for tropopause folding of PV anomalies induced by surface frontal collapse. *Q. J. R. Meteorol. Soc.* **126**: 2747–2764.

DOI: 10.1002/qj